DOI:

Article type: Full Paper

# Highly Uniform, Self-Assembled AlGaN Nanowires for Self-Powered Solar-Blind Photodetector with Fast-Response Speed and High Responsivity

*Danhao Wang, Chen Huang, Xin Liu, Haochen Zhang, Huabin Yu, Shi Fang, Boon S. Ooi, Zetian Mi, Jr-Hau He, and Haiding Sun**

D. H. Wang, C. Huang, X. Liu, H. C. Zhang, H. B. Yu, S. Fang and Prof. H. D. Sun

School of Microelectronics, University of Science and Technology of China, Hefei, Anhui 230026, China

Email: haiding@ustc.edu.cn

Prof. B. S. Ooi

Computer, Electrical, and Mathematical Sciences and Engineering Division, King Abdullah University of Science and Technology (KAUST), Thuwal 23955-6900, Saudi Arabia

Prof. Z. T. Mi

Department of Electrical Engineering and Computer Science, University of Michigan, 1301 Beal Avenue, Ann Arbor, MI 48109, USA

Prof. J. H. He

Department of Materials Science and Engineering, City University of Hong Kong, Kowloon, Hong Kong SAR, 999077, China

Keywords: AlGaN nanowires, self-power, solar-blind, photoelectrochemical photodetectors

**Abstract**

Searching for power-independent, compact, and highly environment-sensitive photodetectors (PDs) is a critical step towards the realization of next-generation energy-efficient and sustainable integrated optoelectronic system. Particularly, the deep ultraviolet (UV) band, which has large photon energy, is extremely suitable for environment monitoring and invisible light communication application. Herein, the demonstration of self-powered deep UV solar-blind PDs in a configuration of photoelectrochemical (PEC) cell is reported, adopting wide bandgap n-type aluminum gallium nitride nanowires (AlGaN NWs) directly grown on conductive silicon (Si) substrates to serve as photoanode. After decorating nanowires with noble metal ruthenium (Ru) which could drive active redox reactions during PEC process, the

constructed solar-blind PEC PDs exhibited excellent responsivity of 48.8 mA $W^{-1}$, fast response speed (rise time of 83 ms and decay time of 19 ms) with large photocurrent density of 55 μA $cm^{-2}$ at 254 nm illumination without external power supply (zero bias). Such superior performance can be attributed to, firstly and foremost, the successful synthesis of highly uniform and defect-free n-type AlGaN NWs which ensures efficient photogeneration via effective light-harvesting, and secondly, the boosted carrier separation and collection efficiency with the help of Ru decoration on nanowire's surfaces. This novel architecture of AlGaN: Ru NW PEC PDs enables deep UV photodetection to work stably with low energy consumption, intriguingly, opening the possibility for the development of high-performance PEC-type PDs based on group III-nitride semiconductors (InN, GaN, AlN) covering the entire spectral range from infrared to deep UV.

## Introduction

Constructing self-powered devices that can work independently, wirelessly, and sustainably without external power supply emerges as a significant research topic for the next-generation electronic systems.[1-3] Self-powered photodetectors (PDs), as one of the key family members in an energy-efficient optoelectronic sensing system, attract huge attention in past few years.[4-6] Typical architectures of self-powered PDs are divided into p-n junction type, Schottky junction type, and photoelectrochemical (PEC) type.[7-9] Among them, PEC PDs exhibit a list of merits, including easy-to-fabricate process, low cost, excellent responsivity, and fast photoresponse,[10-12] therefore being extensively investigated to construct highly efficient self-powered PDs.

It should be noted that previous investigations of PEC PDs mainly focused on visible spectral range and ultraviolet (UV) spectral range (~360 nm), while there were limited studies on solar-blind (~250 nm) detection,[9, 10] which is particularly suitable for light detection in harsh, remote, and aqueous environment, such as submarine oil leakage and ozone monitoring, biological/chemical detection and ultraviolet spectroscopy analysis, as well as invisible light communication system.[12-15] Therefore, searching for

semiconductors with larger bandgaps is the prerequisite to the realization of self-powered solar-blind PEC PDs. By alloying binary gallium nitride (GaN) with aluminum nitride (AlN) and tuning their compositions, we can synthesis ternary aluminum gallium nitride ($Al_xGa_{1-x}N$: $0 \le x \le 1$) as photoanodes which can cover a wide UV detection spectral range (210-360 nm).[16, 17] Moreover, the advantages of high carrier mobility and extremely chemical stability of $Al_xGa_{1-x}N$ material system make AlGaN-based PEC PD perfectly suited to the applications of the sensitive solar-blind detection in harsh aqueous environment.

Additionally, for PEC cell, the electrolytes are crucial components for achieving the electronic circuit, providing ionic conductivity between the working electrode and counter electrode.[18, 19] Conventionally, the $I^-/I_3^-$ redox couple (ionic liquid) was used as the electrolyte.[8, 10] However, owing to the strong volatility, corrosivity, and latent interaction with metallic components, $I^-/I_3^-$ ionic liquid gravely limits the long-term operation of PEC PDs, thus their short lifespan and poor stability become the biggest bottlenecks for practical applications.[9] In recent years, aqueous solution has been explored as the

electrolyte to build PEC PDs, due to its safe, stable, and environmental-friendly characteristics. Unfortunately, previous aqueous PEC PDs have inferior responsivity and photoresponse compared with $I^-/I_3^-$-type,[11, 20, 21] mainly due to the poor material quality resulting in severe trapping and recombination of photoexcited carriers, as well as the low catalytic activity of reaction sites which limits the electrochemical process and further affects device performance. Consequently, the surface decoration of high-quality semiconductors using well-designed co-catalysts is vitally significant for the performance improvement of PEC PDs.

In this context, we demonstrate the self-powered solar-blind PEC-type PDs based on n-type AlGaN nanowires (NWs) grown by molecular beam epitaxy (MBE) on the conductive Si substrate and the growth conditions follow our previous recipe.[22] These vertically-aligned, spontaneously formed NWs are particularly attractive for photodetection purposes owing to (1) their large surface-to-volume ratio for unambiguously enhanced light absorption and (2) their high crystalline quality that is free of dislocations and defects for sufficient photogeneration, effective separation and fast

transport of carriers. Thereafter the nanowire growth, in analogous to visible-light PEC artificial photosynthesis by loading co-catalyst on the surface of semiconductor,[23, 24] we decorated the AlGaN NWs using novel metal ruthenium (Ru) which could drive the active redox reactions during PEC process and subsequently fabricated the entire AlGaN: Ru NWs as the photoanode for solar-blind photodetection test. Intriguingly, the solar-blind PEC PDs exhibits an extremely large photocurrent density of 55 μA $cm^{-2}$ with a record-high responsivity of 48.8 mA $W^{-1}$ under 254 nm illumination at zero bias. Furthermore, the device features a record fast response/recovery time of 83/19 ms, which has never been previously achieved in other self-powered solar-blind PEC PDs. These superior performance reveals that the AlGaN: Ru nanostructure is a promising candidate for self-powered, high-sensitivity solar-blind photodetection application with low cost, large scalability, and excellent stability.

## Results and Discussion

The detailed morphology of the AlGaN: Ru NWs were discerned using scanning electron microscopy (SEM) and transmission electron microscopy (TEM). The SEM images of the AlGaN NWs captured at a tilt angle of 30° are shown in Figure 1a and Figure S1. The as-grown NWs are almost vertically aligned on the planar (001) Si substrate with relative uniform diameters of ~55 nm and lengths varying from 180 to 200 nm. The TEM characterization in Figure 1b and Figure S2 demonstrate the intact appearance of a single nanowire. As the high-resolution transmission electron microscopy (HRTEM) image shows in Figure 1b inner, the fringe lattice parameter of the AlGaN nanowire was determined as 5.167 Å, which can be assigned to the lattice spacing between the two adjacent (0001) plane,[25] suggests the growth direction along the c-axis.

Through the above morphology characterizations, however, no obvious Ru-related nanoparticles were observed. To further investigate the interaction between Ru species and AlGaN NWs after photodeposition, the photoluminescence (PL) measurements were performed (Figure 1e). Under an excitation wavelength of 266 nm at room temperature,

the PL peaks of two samples are centered at 320 nm which indicates the AlGaN NWs possess about 25% Al composition calculated by the following formula:

$$E_g(Al_xGa_{1-x}N) = xE_g(AlN) + (1-x)E_g(GaN) - bx(1-x)$$

where $b$ is the bowing parameter given 0.98 eV.[26]

In principle, the recombination of electrons and holes in direct-bandgap semiconductors, have the same crystal momentum, excluding the involvement of phonons in the recombination process.[27] The intensity of PL peaks is indicative of the amounts of photons generated from radiative recombination of photo-generated carriers. The steady-state PL peak of AlGaN: Ru NWs was significantly suppressed with respect to those of pristine AlGaN NWs. It could be explained by the fact that the metal Ru could allow smooth charge migration from the photoexcited semiconductor, according to the built-in electric field at the interface that results from the alignment of the potentials of the Ru and AlGaN nanowires. [28-30] In other words, the decoration of Ru species reduces the possibility of radiative electron-hole recombination, promoting the photocarrier separation with respect to the pristine AlGaN nanowires.

To further determine the distribution of the Ru species, scanning transmission electron microscopy (STEM) characterization was carried out. Energy dispersive spectroscopy (EDS) mapping analysis of the STEM images revealed the homogeneous dispersion of Ru species in AlGaN: Ru NWs (Figure 1c,d). Therefore, it is concluded that the Ru species are loaded adequately on the surface of NWs. In order to examine the valence state of Ru species loaded on the nanowire surface, the X-ray photoelectron spectra (XPS) survey spectra of the AlGaN: Ru samples are exhibited in Figure 1f and Figure S3. All binding energies were calibrated by the C 1s peak (284.6 eV) arising from adventitious carbon. Due to the loading quantity at a minute magnitude, the Ru 3d signals were covered by C 1s peak. However, in the captured Ru 3p spectrum (Figure S3), the peak at 463.0 eV is different from the typical peaks at 461.2 eV for Ru metal, which has been likely attributed to the presence of an oxidation state close to Ru(III) or Ru(IV).[31] In N 1s (Figure 1f) spectra of AlGaN: Ru NWs and bare AlGaN NWs, the peaks at 397.1 and 398.0 eV can be consistent with the value of Al–N and Ga–N bonds respectively,[32] and the 398.6 eV, which does not appear in N 1s spectrum of bare

AlGaN NWs, is assigned to Ru-N bond.[33] The XPS analysis unambiguously prove the strong interaction between Ru and AlGaN NWs. Together with above PL, STEM-EDS mapping results, we can confirm that the Ru co-catalysts were successfully anchored to the AlGaN nanowire surface.

Figure 2 shows the schematic illustration for measuring the photodetection characteristics of the AlGaN: Ru NW PEC PDs by using the three-electrode system. First, the n-AlGaN: Ru NW samples were fabricated as the photoanodes and then loaded in PEC cell for photodetection measurement. In theory, when an n-type semiconductor is in contact with electrolyte, it would exhibit an upward band bending at the AlGaN/electrolyte interface due to the transport of electrons from the semiconductor to the electrolyte to achieve electrochemical equilibrium (as shown in Figure 2 inner).[18] In this case, when external UV illumination is applied, the photoexcited holes are more likely to transport to the AlGaN/electrolyte interface. Driven by Ru co-catalysts at the interface, holes are captured by hydroxide ions to undergo redox reactions to form redox molecules ($h^+ + OH^- \rightarrow OH^*$). Meanwhile, electrons drift into AlGaN NWs and flow through the external

circuit to Pt counter electrode. Thereafter, the redox molecules, which diffuse through the $H_2SO_4$ electrolyte to the surface of the Pt counter electrode, are reduced to hydroxide ions with the help of electrons re-entered from the external circuit ($e^- + OH^* \rightarrow OH^-$), completing the current loop.[34-36] The Ag/AgCl electrode serves as the reference electrode which has a stable and well-known electrode potential. Its only role is to act as a reference in measuring and controlling the working electrode's potential and at no point does it pass any current and undergo chemical reactions. The electron flow throughout the PEC photodetection circuit can be clearly observed in Figure 2. It is worth mentioning that, during the PEC operation process, the upward surface band bending can lead to majority of photoexcited holes to gather at the surface of semiconductors, possibly resulting in oxidation metamorphism,[37, 38] namely the photo-corrosion effect. In this regard, the Ru co-catalysts can help drive the photoexcited holes into reaction sites to participate in redox reactions instead of etching the semiconductor material itself,[39] effectively alleviating such unedifying photo-corrosion.

To validate the conductivity type of the AlGaN NWs, we first conducted the open circuit potential (OCP) measurement under periodically switching illumination with different wavelength (λ = 254, 365, 254+365 nm) in 0.01 M $H_2SO_4$, as presented in the top of Figure 3a. The observed negative shift of the OCP behavior illustrates the n-type conductivity of our AlGaN NWs. This can be explained as: under UV illumination, the n-type AlGaN NWs would absorb photons and generate free minority carriers which shift the electron quasi-Fermi level upward and flatten the band at the AlGaN/electrolyte interface.[40] Therefore, the OCP measurements would exhibit a negative shift, which confirms the n-type conductivity of the grown samples. Furthermore, ΔOCP (the difference between OCP in the dark/light conditions) reflects the steady-state photogenerated carrier concentration.[40] The lower ΔOCP indicates negligible light absorption at 365 nm wavelengths, compared to direct bandgap transition under 254 nm irradiation, suggesting the high potential of n-AlGaN NWs for solar-blind detection. Thus, to evaluate the corresponding solar-blind detection performance of the AlGaN: Ru nanostructures, we measured time-dependent photocurrent ($I_{photo}$) of AlGaN: Ru NWs at

fixed 0.93V bias under same irradiation condition, shown in the bottom of Figure 3a. Here we define $I_{photo}$ using the following equations:

$$I_{photo} = I_{light} - I_{dark}$$

Where $I_{light}$ is the light current, the $I_{dark}$ is the dark current. The device exhibits an obvious photoresponse with the periodic illumination at 30 s interval. Just same as OCP test, the photocurrent exhibits sensitive dependence on the incident wavelength. The calculated photocurrent density is 152 μA $cm^{-2}$ at 254 nm (solar-blind) compared to 3 μA $cm^{-2}$ at 365 nm (UV). Therefore, both the OCP and photocurrent tests illustrate that the photoexcitation is dominated by the direct transitions (electrons in the semiconductor are excited from the occupied valence band to the unoccupied conduction band), indicating AlGaN: Ru NW PEC PDs are promising candidates for solar-blind detection.

As the operation of PEC PD strongly depends on the external condition, it offers us alternative tunability compared to traditional solid-state PD. Therefore, we subsequently investigate the dependence of external bias on the device performance. At 1.15 mW $cm^{-2}$ illumination, the photocurrent density with varying bias voltage in 0.01 M $H_2SO_4$ is plotted.

As shown in Figure 3b, the photocurrent density of as-prepared AlGaN: Ru NW photoanodes demonstrates a steady increase when the applied bias is raised. The photocurrent density is 149 μA $cm^{-2}$ for 0.8 V, which is 2.7 times higher than 55 μA $cm^{-2}$ for 0 V. This could be attributed to the fact that the applied bias voltage across the photoanode would construct the increasing potential gradient within AlGaN: Ru NWs and promote the separation of photoexcited holes and electrons, suggesting that optimization of photodetection performance can be legitimately modulated by bias voltage in our device.[41] Impressively, the PEC-type PD performs an obvious switching behavior under 0 bias, indicating its potential in self-powered device applications. To further study the impact of electrolyte concentration on the device performance, the photoresponse switching behaviors at different $H_2SO_4$ concentration are compared in Figure 3c.

With 1.15 mW $cm^{-2}$ illumination, the photocurrent of the device increases in 0.05 and 0.1 M $H_2SO_4$ electrolyte, but sharply reduces in 0.5 M $H_2SO_4$ electrolyte. Such phenomenon can be rationally explained by considering that the increase in the concentration of protons enhances the conductivity of the electrolyte, but it also inhibits the oxidation half

reaction: ($h^+ + OH^- \rightarrow OH^*$) at the photoanode/electrolyte interface. From the above analysis we can conclude that this system is more suitable for a weak acid aqueous environment. As critical indicators to judge how fast it responses to external illumination, we investigated the response and recovery characteristics of the device, as shown in Figure 3d. The rise time ($t_r$) refers to the time required for the photocurrent to increase from 10% to 90% of the maximum value and the decay time ($t_d$) refers to the time required for the photocurrent to recover from 90% to 10% of the maximum value. The corresponding $t_r$ of 83 ms and $t_d$ of 19 ms indicate the high photoresponse speed of this PD. Early reports have shown that the solution concentration in the electrolyte has a great influence on the photoresponse speed of PEC type photodetector[20-21]. Thus the rising and decay time could highly depends on the $H_2SO_4$ concentration in this study which requires further optimization.

To analyze the quantitative dependence of the photocurrent on the illumination intensity, the time-dependent photoresponse under different illumination power is presented in Figure 4 a. The measured photocurrent density at 0 bias as a function of illumination

power intensity is plotted in Figure 4 b (red triangles), in which the photocurrent density is 5.86 μA $cm^{-2}$ at 0.2 mW $cm^{-2}$ and linearly increases to 71.5 μA $cm^{-2}$ at 1.5 mW $cm^{-2}$, indicating that the photoexcited electron-hole pairs are effectively separated and can hardly be captured by trap states.[42] Here, we define responsivity (R) as the photocurrent generated by unit power of the incident light on the effective area, namely

$$R = \frac{I_{photo}}{P_{inc}}$$

where $P_{inc}$ is the incident light power density. The calculated maximum R (blue circles in Figure 4b) of the self-powered AlGaN: Ru NW PEC PD is 48.8 mA $W^{-1}$ under the 254 nm light irradiation with the incident light intensity of 1.5 mW $cm^{-2}$. Such value is superior to most PEC-type UV PDs made by oxide-based nanostructures (see Table S1 for details).[43-49] The extraordinary performance should be attributed to (1) the highly uniform AlGaN nanowire structure which possesses large light absorption capability, ensuring the high irradiation utilization; (2) the MBE-grown AlGaN materials with high crystalline quality enabling sufficient carrier photogeneration and trap-free carrier transport; (3) the high catalytic activity of Ru decoration which helps drive the photoexcited carriers to

redox reaction sites, thus promoting the carrier separation and alleviating the photo-corrosion of AlGaN nanowire surface. Furthermore, to testify the robustness of the experimental conditions, we execute an additional measurement of photocurrents under 0.4 V for 600 s. The device exhibits excellent stability in terms of on/off switching during the test, as shown in Figure 4c, indicating the reliability and accuracy of all the performed measurements.

For a better comparison of the solar-blind photodetection ability, Figure 4d plots the device performance of the newly designed PEC PDs in this work and recently reported self-powered solar-blind PEC PDs with nanostructure photoelectrodes based on wide bandgap oxides and sulfides.[12,34-36] Obviously, our proposed AlGaN: Ru NW PEC PD shows ever-reported fastest photoresponse speed and highest responsivity, revealing the great potential of such device architectures in the field of the high-efficiency solar-blind PEC photodetection. Moreover, the device performance of AlGaN: Ru NW PEC PDs depends not only on the excitation and transport of carriers within the semiconductor itself, but also on the diffusion of ions in the aqueous environment, which

provide us a new method to modulate the photodetection performance to meet desired requirements.

**Conclusion**

In summary, we have explored the first self-powered solar-blind PEC PD based on highly-uniform n-AlGaN NWs grown by the MBE technique. Ru co-catalysts were used to decorate the surface of NWs to ensure that device performance would not be hampered by insufficient chemical activity during PEC photodetection. The PEC PD performance can be readily modulated by varying external experimental conditions, for instance, bias voltage, light source wavelength, light power density and electrolyte properties. The photoresponse characteristics of the fabricated self-powered PEC UV PD were investigated systematically. A large photocurrent density of 55 μA $cm^{-2}$ and excellent responsivity of 48.8 mA $W^{-1}$ at 254 nm illumination, together with extraordinary fast response speed (rise time of 83 ms and decay time of 19 ms) were measured, which are superior to ever-reported self-powered solar blind PEC PDs made of oxide and sulfide-based nanostructures. This work confirms the feasibility of III-nitride NWs as excellent

photoanodes to achieve highly sensitive and stable photodetection and demonstrates great prospects to realize highly efficient self-powered PDs for compact energy harvesting nanosystems in the near future.

## Experiment Section

The n-type AlGaN NWs were grown on Si (100) substrates using a Veeco plasma-assisted molecular beam epitaxy (PAMBE). Before the Si wafer was loaded into the MBE chamber, the surface oxide on the wafer was removed using the HF-$H_2O$ solution. After cleaning, the Si wafer was then outgassed in the load-lock chamber at 200 °C for 1 h followed by outgassing in the buffer chamber at 650 °C to remove any water components and organic-based contaminants. For the nanowire growth, the Si-doped GaN seeds were first nucleated on top of the Si wafer at ~500 °C for 1 min to reduce Ga adatom desorption and increase the nucleation probability. The nitrogen plasma source was operated with a flow rate of 1.0 standard cubic centimeter per minute (sccm) and RF-power of 300 W and metal source are supplied by standard Knudsen cell with beam

equivalent pressure (BEP) values of (Ga) 6.0 × $10^{-8}$ Torr. The k-cell temperature of Si dopant is 1180 °C. After the nucleating layer of less than 3 nm n-GaN was grown, the temperature was then increased to 630 °C to grown the n-AlGaN layer for 2 hours with Al and GaN BEPs of 5 × $10^{-8}$ and 9 × $10^{-8}$ Torr, respectively, while the Si cell temperature was kept at 1180 °C with the same nitrogen plasma condition.

PL measurements were measured by an OceanOptics QEPro spectrometer, performed to investigate the optical properties of the nanowire samples (using 266 nm laser as the excitation source). The morphology of the AlGaN NWs was characterized using field emission scanning electron microscopy (FESEM) on Hitachi, SU8220 systems at an accelerating voltage of 3 kV. TEM, EDS, and high-angle annular dark-field scanning transmission electron microscopy (HAADF-STEM) measurements were performed on a JEM-ARM200F instrument (Anhui University) with probe corrector operating at an acceleration voltage of 300 kV. The TEM specimens were prepared by focused ion beam (FIB). XPS was acquired on the Photoemission End station at the BL10B beamline in the National Synchrotron Radiation Laboratory (NSRL) in Hefei, China.

Before the PEC measurement, Ru co-catalysts were in-situ photodeposited from an aqueous $RuCl_3$ (10 mg/mL) solution for introducing active sites on the nanowire surface to accelerate the redox reaction (see Supporting Information S1 for details). The PEC experiments were conducted in a typical three-electrode cell. Pt mesh and Ag/AgCl were utilized as the counter electrode and reference electrode, respectively. The PEC cell was made of quartz with good transmittance for both visible and UV light. For the working electrode, Ga-In eutectic alloy (Alfa Aesar) was first deposited on the backside of the Si substrate to form an ohmic contact, which was subsequently connected with a copper sheet using silver paste. The entire photoanode device, except the nanowire surface ($5\times5$ $mm^2$), was then covered with an insulating epoxy to avoid any leakage current. The photoanodes were dried at room temperature in air for at least 24 h before measurement. A 0.01 M $H_2SO_4$ was used as the electrolyte instead of an alkaline solution since the alkali would readily corrode III-nitride materials.[50] A Tanon UV-100 lamp was used to generate 254/365 nm monochromatic deep UV light and the light intensity was calibrated by an optical power meter (S401C and PM100D).

AUTHOR INFORMATION

**Corresponding Author**

*Email: haiding@ustc.edu.cn;

**ORCID**

Danhao Wang: 0000-0001-5242-177X

Chen Huang: 0000-0003-3350-0805

Haochen Zhang: 0000-0001-7664-9074

Huabin Yu: 0000-0003-2487-2076

Shi Fang: 0000-0001-9255-1579

Haiding Sun: 0000-0001-8664-666X

## Supporting Information

Supporting Information is available from the Wiley Online Library or from the author.



## Acknowledgements

D. H. W. and C. H. contributed equally to this work. This work was funded by National Natural Science Foundation of China (Grant No. 61905236), University of Science and Technology of China (Grant No. KY2100000081), Chinese Academy of Sciences (Grant No.KJ2100230003), the Fundamental Research Funds for the Central Universities (Grant No. WK2100230020), USTC Research Funds of the Double First-Class Initiative (Grant No. YD3480002002), USTC National Synchrotron Radiation Laboratory (Grant No. KY2100000099) and was partially carried out at the USTC Center for Micro and Nanoscale Research and Fabrication. We thank Prof. Binghui Ge from Anhui University for the support of TEM characterization.

## Author contributions

H.D.S. developed the idea and H.D.S., B.S.O., Z.T.M., and J.H.H. discussed the experiments. D.H.W., C.H., X.L., H.C.Z., H.B.Y. and S.F. fabricated the photocathode and performed the characterizations and photoelectrochemical experiments, collected, and analyzed the data. C.H., D.H.W., and X.L. performed photodeposition synthesis. D.H.W. and H.D.S. performed the STEM characterization. D.H.W., C. H. and H.D.S. wrote the initial draft of the paper and the manuscript was revised by other co-authors. All authors discussed the results and commented on the manuscript.

## Conflict of Interest

The authors declare no conflict of interest.

## References

[1] X. Liu, H. Gao, J.E. Ward, X. Liu, B. Yin, T. Fu, J. Chen, D.R. Lovley, J. Yao, *Nature* **2020**, 578, 550.

[2] S. Park, S.W. Heo, W. Lee, D. Inoue, Z. Jiang, K. Yu, H. Jinno, D. Hashizume, M. Sekino, T. Yokota, K. Fukuda, K. Tajima, T. Someya, *Nature* **2018**, 561, 516.

[3] S. Wang, J. Xu, W. Wang, G.N. Wang, R. Rastak, F. Molina-Lopez, J.W. Chung, S. Niu, V.R. Feig, J. Lopez, T. Lei, S.K. Kwon, Y. Kim, A.M. Foudeh, A. Ehrlich, A. Gasperini, Y. Yun, B. Murmann, J.B. Tok, Z. Bao, *Nature* **2018**, 555, 83.

[4] H. Sun, W. Tian, F. Cao, J. Xiong, L. Li, *Adv. Mater.* **2018**, 30, 1706986.

[5] D. Xiang, C. Han, Z. Hu, B. Lei, Y. Liu, L. Wang, W.P. Hu, W. Chen, *Small* **2015**, 11, 4829.

[6] Y. Chen, C. Wang, G. Chen, Y. Li, C. Liu, *Nano Energy* **2015**, 11, 533.

[7] C. Zhou, S. Raju, B. Li, M. Chan, Y. Chai, C.Y. Yang, *Adv. Funct. Mater.* **2018**, 28, 1802954.

[8] W. Tian, Y. Wang, L. Chen, L. Li, *Small* **2017**, 13, 1701848.

[9] L. Su, W. Yang, J. Cai, H. Chen, X. Fang, *Small* **2017**, 13,1701687.

[10] J. Zhou, L. Chen, Y. Wang, Y. He, X. Pan, E. Xie, *Nanoscale* **2016**, 8, 50.

[11] Z. Xie, C. Xing, W. Huang, T. Fan, Z. Li, J. Zhao, Y. Xiang, Z. Guo, J. Li, Z. Yang, B. Dong, J. Qu, D. Fan, H. Zhang, *Adv. Funct. Mater.* **2018**, 28, 1705833.

[12] D. Li, S. Hao, G. Xing, Y. Li, X. Li, L. Fan, S. Yang, *J. Am. Chem. Soc.* **2019**, 141, 3480.

[13] C. Xie, X. Lu, X. Tong, Z. Zhang, F. Liang, L. Liang, L. Luo, Y. Wu, *Adv. Funct. Mater.* **2019**, 29, 1806006.

[14] X. Hou, H. Sun, S. Long, G. S. Tompa, T. Salagaj, Y. Qin, Z. Zhang, P. Tan, S. Yu, M. Liu, *IEEE Electron Device Lett.* **2019**, 40, 1483-1486.

[15] D. Zhang, W. Zheng, R. Lin, Y. Li, F. Huang, *Adv. Funct. Mater.* **2019**, 29, 1900935.

[16] M. Kneissl, T. Seong, J. Han, H. Amano, *Nat. Photonics* **2019**, 13, 233.

[17] C. Z. Ning, L. Dou, P. Yang, *Nat. Rev. Mater.* **2017**, 2, 1.

[18] M. Gratzel, *Nature* **2001**, 414, 338.

[19] K. Sivula, R. Van De Krol, *Nat. Rev. Mater.* **2016**, 1, 15010.

[20] X. Ren, Z. Li, Z. Huang, D. Sang, H. Qiao, X. Qi, J. Li, J. Zhong, H. Zhang, *Adv. Funct. Mater.* **2017**, 27, 1606834.

[21] Z. Li, H. Qiao, Z. Guo, X. Ren, Z. Huang, X. Qi, S.C. Dhanabalan, J.S. Ponraj, D. Zhang, J. Li, J. Zhao, J. Zhong, H. Zhang, *Adv. Funct. Mater.* **2018**, 28, 1705237.

[22] B. Janjua, H. Sun, C. Zhao, D.H. Anjum, F. Wu, A.A. Alhamoud, X. Li, A.M. Albadri, A.Y. Alyamani, M.M. El-Desouki, *Nanoscale* **2017**, 9, 7805.

[23] Y. Cao, D. Wang, Y. Lin, W. Liu, L. Cao, X. Liu, W. Zhang, X. Mou, S. Fang, X. Shen, T. Yao, *ACS Appl. Energy Mater.* **2018**, 1, 6082-6088.

[24] S. Vanka, E. Arca, S. Cheng, K. Sun, G.A. Botton, G. Teeter, Z. Mi, *Nano Lett.* **2018**, 18 6530.

[25] S. Kang, R. Nandi, H. Kim, K. U. Jeong, C. R. Lee, *J. Mater. Chem. C* **2018**, 6, 1176.

[26] K. Yamano, K. Kishino, H. Sekiguchi, T. Oto, A. Wakahara, Y. Kawakami, *J. Cryst. Growth* **2015**, 425, 316.

[27] L. Zhang, J. Ran, S. Z. Qiao, M. Jaroniec, *Chem. Soc. Rev.* **2019** 48, 5184.

[28] W. Liu, L. Cao, W. Cheng, Y. Cao, X. Liu, W. Zhang, X. Mou, L. Jin, X. Zheng, W. Che, Q. Liu, T. Yao, S. Wei, *Angew. Chem., Int. Ed.* **2017**, 56, 9312.

[29] Y. Cao, S. Chen, Q. Luo, H. Yan, Y. Lin, W. Liu, L. Cao, J. Lu, J. Yang, T. Yao, S. Wei, *Angew. Chem., Int. Ed.* **2017**, 56, 12191.

[30] S. Chen, T. Takata, and K. Domen, *Nat. Rev. Mater.* **2017** 2, 1-17.

[31] C. Zhang, J. Sha, H. Fei, M. Liu, S. Yazdi, J. Zhang, Q. Zhong, X. Zou, N. Zhao, H. Yu, Z. Jiang, E. Ringe, B.I. Yakobson, J. Dong, D. Chen, J.M. Tour, *ACS Nano* **2017**, 11, 6930.

[32] R. Jiang, X. Meng, *J. Mater. Sci.: Mater. Electron.* **2019**, 30,16266.

[33] L. Zeng, H. Peng, W. Liu, J. Yin, L. Xiao, J. Lu, L. Zhuang, *J. Power Sources* **2020**, 461, 228147.

[34] J. Zhang, S. Jiao, D. Wang, S. Ni, S. Gao, and J. Wang, *J. Mater. Chem. C* **2019** 7, 6867.

[35] K. Chen, S. Wang, C. He, H. Zhu, H. Zhao, D. Guo, Z. Chen, J. Shen, P. Li, A. Liu, and C. Li, *ACS Appl. Nano Mater.* **2019** 2, 6169.

[36] C. He, D. Guo, K. Chen, S. Wang, J. Shen, N. Zhao, A. Liu, Y. Zheng, P. Li, Z. Wu, and C. Li, *ACS Appl. Nano Mater.* **2019** 2, 4095.

[37] M. Kibria, S. Zhao, F. A. Chowdhury, Q. Wang, H. P. T. Nguyen, M. L. Trudeau, H. Guo, Z. Mi, *Nat. Commun.* **2014**, 5, 1.

[38] M. Kraut, F. Pantle, J. Winnerl, M. Hetzl, F. Eckmann, I.D. Sharp, M. Stutzmann, *Nanoscale* **2019**, 11,7967.

[39] J. Kamimura, P. Bogdanoff, J. Lähnemann, C. Hauswald, L. Geelhaar, S. Fiechter, H. Riechert, *J. Am. Chem. Soc.* **2013**, 135, 10242.

[40] J. Kamimura, P. Bogdanoff, M. Ramsteiner, P. Corfdir, F. Feix, L. Geelhaar, H. Riechert, *Nano Lett.* **2017**, 17,1529.

[41] Y. Zhang, F. Zhang, Y. Xu, W. Huang, L. Wu, Y. Zhang, X. Zhang, H. Zhang, *Adv. Funct. Mater.* **2019**, 29, 1906610.

[42] L. Zeng, L. Tao, C. Tang, B. Zhou, H. Long, Y. Chai, S.P. Lau, Y.H. Tsang, *Sci. Rep.* **2016**, 6, 20343.

[43] O. Game, U. Singh, T. Kumari, A. Banpurkar, S. Ogale, *Nanoscale* **2014**, 6, 503.

[44] Y. Han, C. Fan, G. Wu, H. Z. Chen, M. Wang, *J. Phys. Chem. C* **2011**, 115, 13438.

[45] L. Chen, X. Li, Y. Wang, C. Gao, H. Zhang, B. Zhao, F. Teng, J. Zhou, Z. Zhang, X. Pan, *J. Power Sources* **2014**, 272, 886.

[46] Q. Li, L. Wei, Y. Xie, K. Zhang, L. Liu, D. Zhu, J. Jiao, Y. Chen, S. Yan, G. Liu, *Nanoscale Res. Lett.* **2013**, 8, 415.

[47] C. Cao, C. Hu, X. Wang, S. Wang, Y. Tian, H. Zhang, *Sens. Actuators, B* **2011**, 156, 114.

[48] Y. Xie, L. Wei, G. Wei, Q. Li, D. Wang, Y. Chen, S. Yan, G. Liu, L. Mei, J. Jiao, *Nanoscale Res. Lett.* **2013**, 8, 188.

[49] X. Li, C. Gao, H. Duan, B. Lu, Y. Wang, L. Chen, Z. Zhang, X. Pan, E. Xie, *Small* **2013**, *9*, 2005.

[50] H. Sun, M.K. Shakfa, M.M. Muhammed, B. Janjua, K.-H. Li, R. Lin, T.K. Ng, I.S. Roqan, B.S. Ooi, X. Li, *ACS Photonics* **2017**, 5, 964.

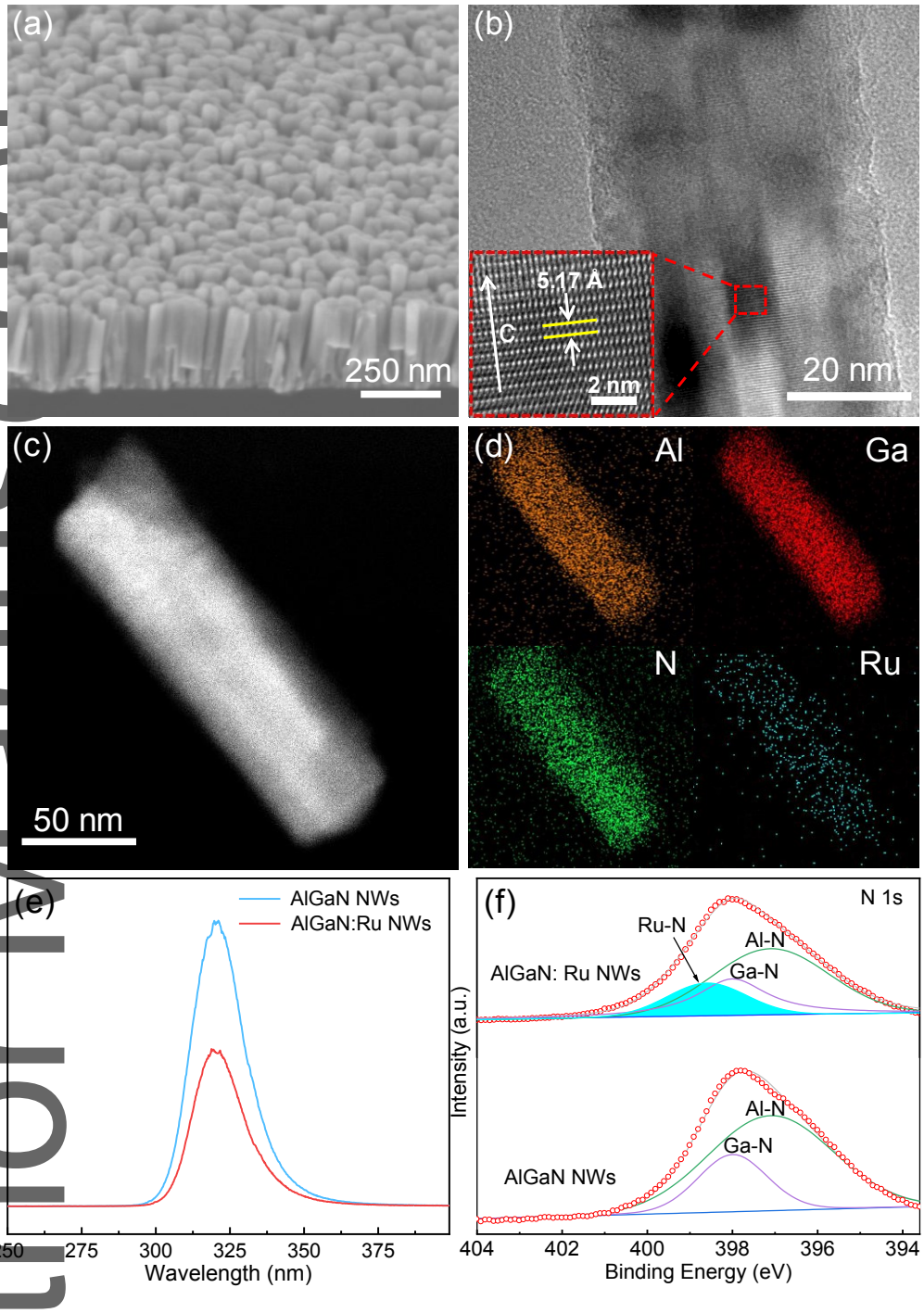

**Figure 1.** a) 30°-tilted SEM image of AlGaN nanowire arrays grown on Si substrate. b) TEM image of a single AlGaN nanowire. Inset is the HRTEM image of the AlGaN nanowire. c) STEM image and d) Elemental mapping of a single AlGaN: Ru nanowire. e) PL spectra of bare AlGaN NWs and AlGaN: Ru NWs at 300K. f) XPS N 1s spectra of AlGaN: Ru NWs and bare AlGaN NWs.

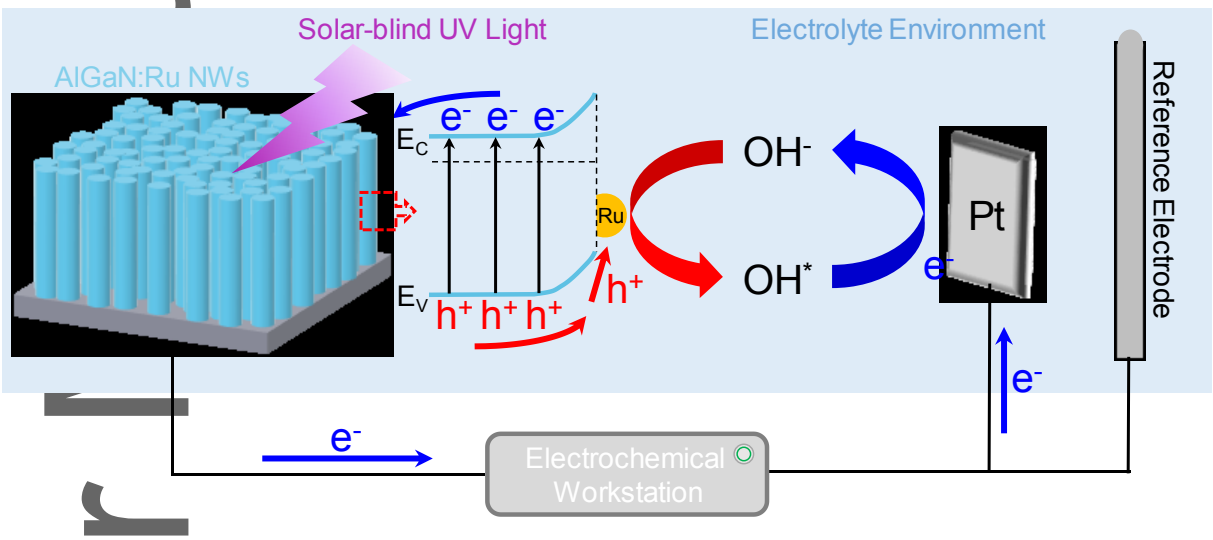

**Figure 2.** Typical three-electrode PEC system built for evaluating the photodetection characteristics of the AlGaN: Ru NW PEC PDs.

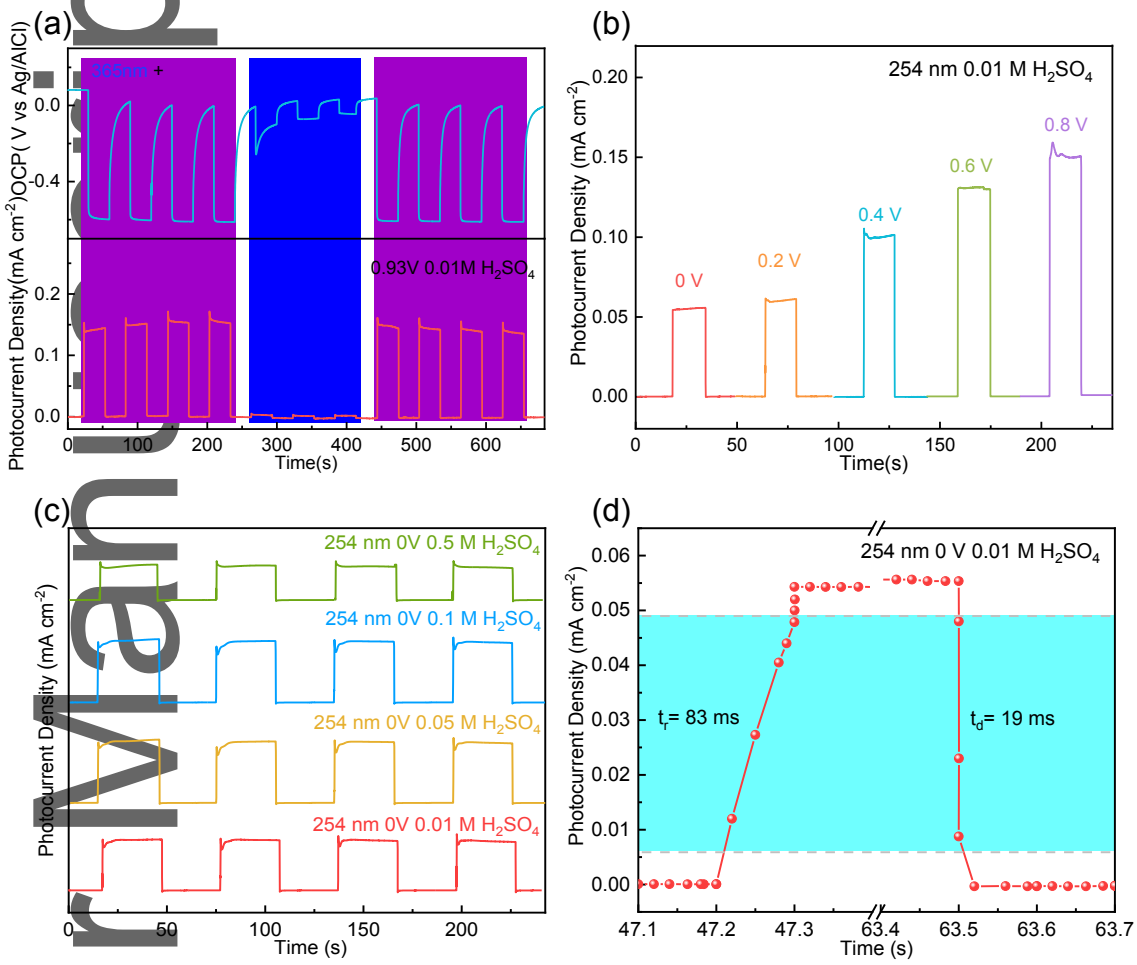

**Figure 3**. a) The time-dependent (top) OCP and (bottom) photocurrent density under 365+254 nm, 365 nm and 254 nm irradiation (1.15 mW $cm^{-2}$), respectively. b) Photocurrent density with various bias voltage (0, 0.2, 0.4, 0.6, 0.8 V). c) Photoresponse switching behaviours with different concentration of $H_2SO_4$ electrolyte (0.01, 0.05, 0.1, 0.5 M). d) Representation of the rise time and decay time interval.

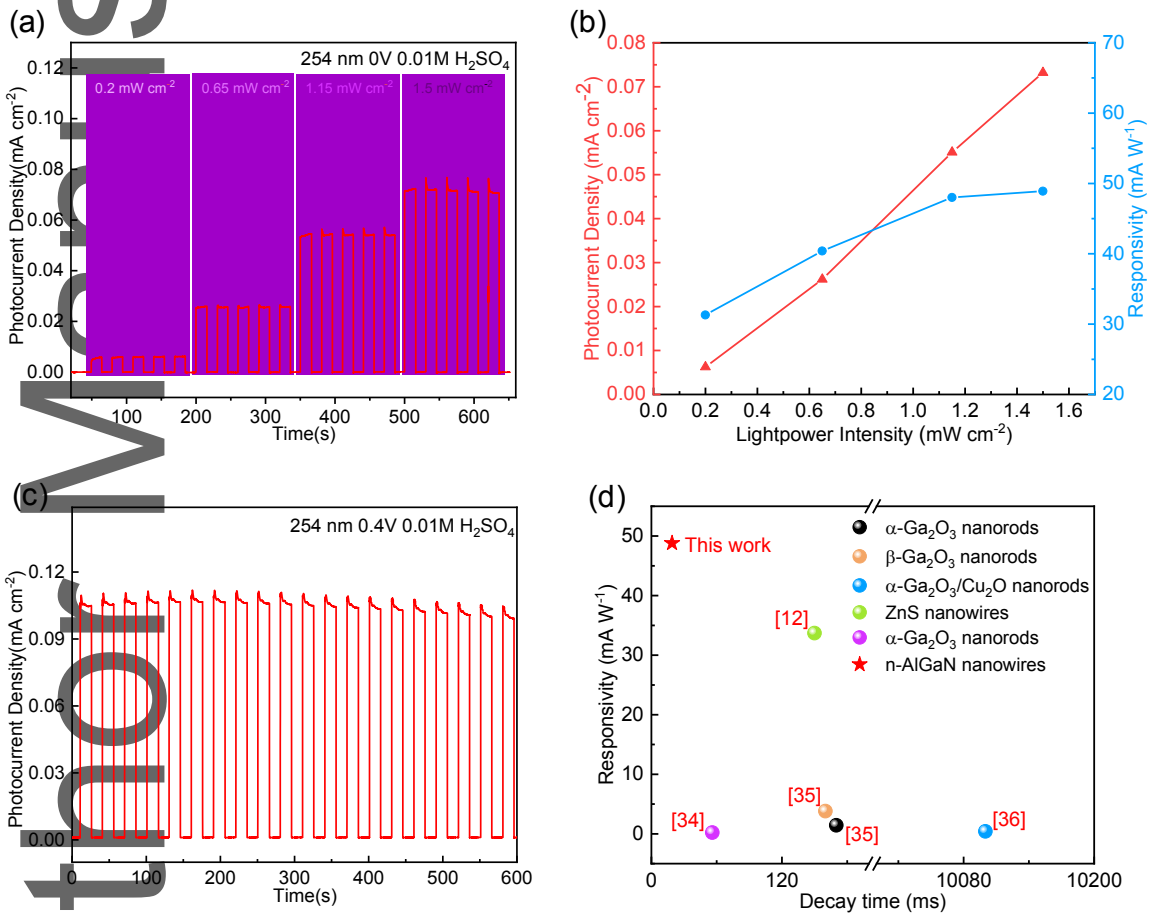

**Figure 4.** a) Photocurrent density of the PD under the incident light intensity of 0.2, 0.65, 1.15, and 1.5 mW $cm^{-2}$. b) Fitting curve and corresponding calculated photoresponsivity of the PD under different light intensities in 0.01 M $H_2SO_4$. c) Long-time photocurrent measurements of the PD under 0.4 V bias potential with 1.15 mW $cm^{-2}$ illumination. d) The comparison of responsivity and recovery speed in previous self-powered solar-blind PEC PDs and this work.

Highly uniform, self-assembled AlGaN nanowires fabricated as self-powered solar-blind photodetector with fast-response speed and high responsivity is demonstrated, in the configuration of photoelectrochemical cell. Owing to the defect-free wide bandgap AlGaN-based nanowires with appropriate surface decoration, the high-performance solar-blind photodetection is realized. Coupled with the self-powered characteristics of photoelectrochemical photodetectors, the proposed novel device architecture unveils an unprecedented opportunity for designing future energy-efficient and sustainable optoelectronic system.

**Keywords**: AlGaN nanowires, self-power, solar-blind, photoelectrochemical photodetectors

*Danhao Wang, Chen Huang, Xin Liu, Haochen Zhang, Huabin Yu, Shi Fang, Boon S. Ooi, Zetian Mi, Jr-Hau He, and Haiding Sun**

**Highly Uniform, Self-Assembled AlGaN Nanowires for Self-Powered Solar-Blind Photodetector with Fast-Response Speed and High Responsivity**

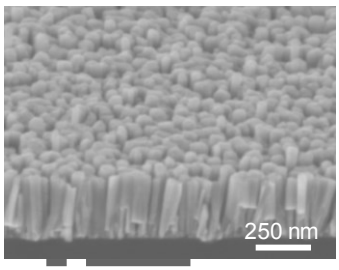


AlGaN: Ru NWs

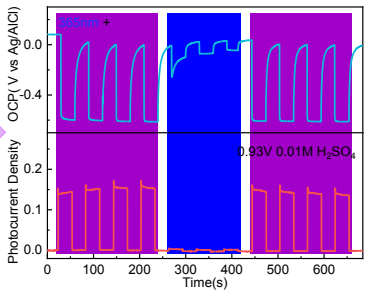


Solar-blind photodetection properties

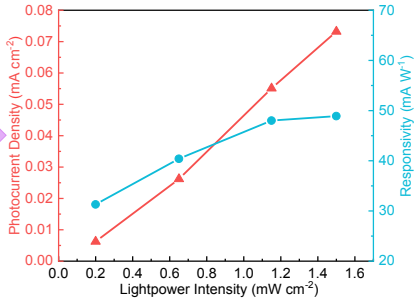


Linear light intensity measurement